DESCRIPTION OF COMPUTER PROGRAM TO SIMULATE WATER INJECTION UNDER INDUCED FRACTURING CONDITIONS

1. INTRODUCTION

1.1. Waterflood fracturing simulator

The purpose of this computer program is to provide via simulation an estimate of lateral and vertical extension of waterflood-induced fractures (both for clean water and produced water injection), of vertical fracture (non-)confinement to target injection zones, of well injectivity, and of the shape and extent of flooded zones. It was developed by merging [1] a number of existing fracturing [2] en waterflooding [3] software packages during the late nineties of last century.

Applications of this program throughout the years have been mainly in the arena of water injection for waterflooding, for reservoir voidage replacement and for (contaminated) water disposal [4-17]. In most of these applications, water injection simulations were carried out to assess issues around fracture containment, sweep and injectivity.

In many waterfloods, fractured water injectors are a common feature. Unintended fracturing in water injectors may occur owing to thermal effects (particularly in offshore areas) or due to pore plugging by impurities in the injection water. Intentional fracturing may be an integral part of the field development plan, since the increased injection potential may enable a significant reduction in the number of injector wells drilled. Furthermore, as a result of fracturing, water purity requirements may be relaxed providing a significant reduction in facilities costs, especially offshore. However, once fracture lengths reach a significant fraction of the well spacing they can have a significant influence on sweep efficiency. Furthermore, if the fracture does not extend over the full height of the formation, non-uniform sweep in the vertical sense may be encountered which may alter field development plans. Finaly, intended or unintended fracturing may lead to out-of-zone growth, particularly when injection rates significantly exceed leakoff rates owing to low formation permeabilities and/or limited disposal storage capacity of the target injection zones. Therefore, the accurate prediction of fracture length and height is required.

Our waterflood fracturing tool computes fracture dimensions, well injectivities, and flood front displacements for water injection under induced fracturing conditions. This applies both to produced water injection and to clean (e.g. sea-)water injection.

2. FRACTURE PROPAGATION: PHYSICAL MECHANISMS INCORPORATED IN THE PROGRAM

2.1. In-situ Stress

The in-situ stress, as it affects hydraulic fracturing, is the local stress state in a given rock mass at depth. The three principal stress components of the local stress state - typically compressive, anisotropic and non-homogeneous - are influenced strongly by the weight of the overburden, burial history, pore pressure, temperature, rock properties, diagenesis, tectonics and visco-elastic relaxation. In addition, drilling, fracturing or production can alter some of these parameters, changing the local stress field.

The stresses control the fracture orientation (vertical or horizontal, and the azimuth of vertical fractures), vertical height growth and containment, surface treating pressures, and internal fracture plugging.

A geological formation in the subsurface that is not partly depleted, is subject to virgin stresses. Firstly, the vertical or maximum stress component σ_1, which equals the weight of the overlying rock mass (overburden) and can easily be obtained from the integration of a density log. If such a log is unavailable a rule of thumb of 1.0 psi/ft (=22.6 kPa/m) is generally a good approximation of this vertical stress component.

This overburden is transmitted into a horizontal stress that, in a tectonically inactive are, will be approximately the same in every direction. Consequently, $\sigma_2 = \sigma_3$ in Fig. 2.1. The general relationship between vertical and horizontal stress uses the principle of effective stress, defined as the stress minus the pore fluid pressure. Hence:

$$\sigma_1' = \sigma_1 - p_f$$

with σ_1'= effective vertical stress
p_f = pore fluid pressure

Sometimes the effective stress is called the grain pressure in the rock matrix.

The following equation provides the effective horizontal stress:

$$\sigma_2' = \sigma_3' = \frac{\nu}{1-\nu}\sigma_1' \quad \text{('Eaton's rule')}$$

with ν = Poisson's ratio

Assuming that $\nu \approx 1/3$, the effective horizontal stress equals approximately one-half of the effective vertical overburden. This value is quite typical for sandstone.

The *total* horizontal stresses follow from the effective horizontal stresses as given below:

$$\sigma_2 = \sigma_3 = \frac{\nu}{1-\nu}(\sigma_1 - p_f) + p_f$$

with σ_1 = total vertical stress (overburden)

For the above example of $\nu = 1/3$, and using σ_1= 1 psi/ft and p_f = 0.45 psi/ft (= 10 kPa/m), one obtains $\sigma_2 = \sigma_3 \approx 0.7$ psi/ft (= 15.8 kPa/m), which is considered a convenient rule of thumb value for tectonically relaxed areas.

Note that the above formulas show that rock layers with higher Poisson's ratio will generally have a higher total horizontal stress. This explains why the horizontal stresses in shales are often higher than in sandstones: shales have a higher Poisson's ratio.

In tectonically active areas, an additional horizontal stress component is present in a certain direction. The result is the intermediate stress (also called 'maximum horizontal stress'), which is normally labelled σ_2. So the following picture emerges: $\sigma_1 > \sigma_2 > \sigma_3$ (Fig. 2.1). The horizontal stresses control the azimuth of the vertical hydraulic frac created, since the frac will orient itself perpendicular to the minimum horizontal stress σ_3 (i.e. it will align itself parallel to the maximum horizontal stress σ_2) to satisfy the minimum energy principle.

More plastic material like shale, anhydrite and rocksalt will transmit more of the vertical stress resulting in a higher horizontal stress. Therefore, if these formations are bounding a reservoir sandstone zone which is being fractured they will contain, partly or completely, the vertical growth of this fracture.

Burial or uplift of the reservoir zone and cementation history, pressurization and depletion will complicate the calculation of the present-day minimum horizontal stress. Consequently, it is essential to measure σ_3 by means of a minifrac procedure, determining the fracture closure pressure (FCP in Fig. 2.2) which equals σ_3.

At shallow depth (typically less than a few hundred metres) the horizontal stresses may be greater than the overburden, due to tectonic stresses, and horizontal fractures will be generated.

2.2. Reservoir depletion / pressurization

During reservoir depletion or pressurization the in-situ stresses change. The total overburden stress will remain constant, but the two total horizontal stresses will decrease (depletion) or increase (pressurization).

If it is assumed that the formation behaves in a linear poro-elastic manner, we can calculate the reduction / increase in the total horizontal stresses using the following equation:

$$\Delta\sigma_2 = \Delta\sigma_3 = A_p \, \Delta p_f$$

where the constant A_p is called the "poro-elastic constant" , which is given by

$$A_p = (1 - \beta)\frac{1 - 2\nu}{1 - \nu}$$

where:

β = ratio of rock grain compressibility to rock matrix compressibility

ν = Poisson's ratio

Δp_f = reduction (depletion) or increase (inflation) of reservoir pressure

The poro-elastic constant A_p can be measured in the laboratory on core samples. For sedimentary basins, values of the poro-elastic constant have been reported between 0.4 and 0.8. The reduction in formation breakdown pressure in Fig. 2.2 (FBP), caused by depletion, can be calculated using the reduced minimum in-situ stresses from above equations. The same approach can be used to correct for the effects of reservoir pressure pressurization.

2.3. Fracture propagation – general

Fracture propagation is governed by the following physical processes (see also Fig. 2.3):

a) Flow of injected fluid towards the fracture tip, giving rise to frictional pressure drop within the fracture (δp_{fric}). When laminar flow is being assumed, the frictional pressure gradient is related to the frac width in the following manner:

$$\frac{\partial p}{\partial r} \propto \frac{\mu Q}{[w(r)]^3}$$

w(r) = 'effective' frac width at distance r from wellbore.

μ = fluid viscosity

Q = injection rate

Note that the 'effective' frac width w(r) incorporates corrections for external filtercake thickness. See under g) below for a further discussion on fracture width versus external filtercake thickness.

b) Elastic opening of the fracture in response to an internal (fluid) pressure distribution. Driving force is the 'net pressure' Δp_w (fig. 2.3), which is equal to the difference between the fluid pressure in the fracture and the total minimum in-situ stress σ_3. For a "long" fracture (i.e. total fracture length > total fracture height), the elastic opening relation is

$$w_{tot} = \frac{2H}{E'} \Delta p_w$$

w_{tot} = 'Total' fracture width, i.e. including the external filtercake
H = total fracture height
E' = 'plane strain' Young's modulus, given by $E' = E/\left(1-\nu^2\right)$, and E the Young's modulus.

Assuming a negligible pressure drop over the perforations and no near-wellbore tortuosity effects, the net pressure Δp_w is given by:

Δp_w = Bottom Hole Pressure (BHP) — Fracture Closure Pressure (FCP)

c) Breaking of the rock at the fracture tip. The resistance of the rock against being fractured can be characterised by a material property, which is called "fracture toughness" (symbol K_{Ic}). Laboratory tests have shown that in order to grow a "large" (length > 0.1m) fracture, a tensile stress T given

$$T = \frac{K_{Ic}}{\sqrt{\pi L}}$$

(L is the fracture length) is required to overcome the rock resistance. It should be noted that for "small" fractures (length < 1 cm), the tensile stress T required to fracture the rock is given by the rock tensile strength. For "intermediate" fractures (1 cm < length < 0.1 m), the growth criterion is somewhere in between these two extremes.

Since hydraulic fractures may be considered as "large", the net propagation pressure Δp_0 is, in the absence of frictional pressure drop, is given by (see also Fig. 2.3b)

$$\Delta p_0 = \frac{K_{Ic}}{\sqrt{\pi L}}$$

Typical lab-measured values for K_{Ic} are in the order of 1 MPa√m (≈ 1000 psi√inch) under unconfined conditions and 3-5 MPa√m (≈ 3000-5000 psi√inch) under confinement typical of reservoir conditions.

d) In-situ stress layering and gradient. The total minimum horizontal in-situ stress $\sigma_3(z)$ is not uniform but in general a function of depth z (Fig. 2.4), characterised by stress "jumps" between different layers in combination with a continuous stress gradient. The example of Fig. 2.4 illustrates the classical situation of a fracture initiated in a sandstone which is bounded on top and on bottom by shale layers. The stress contrast between the top shale layer and the sandstone layer is given by S_1, while the stress contrast between the bottom shale layer and the sand is given by S_2. Moreover, the stress is characterised by a continuous gradient g. As a result of this, the upward and downward growth rate of the fracture will be different from the length-wise growth rate. The stress contrasts tend to "pinch" the fracture width near the top and bottom, and thus inhibit upward and downward growth. On the other hand, the in-situ stress gradient will tend to favour upward growth.

e) Fluid volume balance, which means that fluid pumped into the fracture equals the frac volume plus the leak-off volume. In water injection applications, the fracture volume is generally negligible compared to the leak-off volume.

f) Poro-elastic and thermo-elastic effects during water injection

When water is injected into a hot reservoir, both a cooling of the reservoir and an increase in pressure takes place in the part of the reservoir flooded by water. It can be shown that temperature reduction leads to rock shrinkage, which can result in a noticeable decrease in the total minimum horizontal in-situ stress around the fracture (thermo-elastic stress reduction). The pore pressure increase, on the other hand, results in an increase in the total minimum horizontal in-situ stress around the fracture (poro-elastic stress increase).

Fig. 2.5 shows a schematic picture of a water injection fracture surrounded by zones of different fluid mobility (plan view). Immediately surrounding the fracture, there is an impaired zone, which is caused by 'deep damage' as a result of dirty water injection. This zone will be further discussed under point g) below. The cooled zone is extending beyond the impaired zone. The size of the cooled zone is determined by a heat balance, i.e. the heat absorbed by the (cold) injection water should be equal to the heat transferred by the cooled zone to the cold injection water. Beyond the cooled zone, a warm injection water zone extends, beyond which there is finally the virgin oil (in the case of waterflooding) or aquifer (in the case of disposal into an aquifer).

In our waterflood fracturing program, the poro-elastic and thermo-elastic stress changes are calculated based on the geometry of Fig. 2.5. The equations are:

$$\Delta\sigma_{poro-elastic} = A_p * \left(p_{fracture} - p_f\right) * g_p\left(L, H, B_{flood\ front}\right)$$
$$\Delta\sigma_{thermo-elastic} = A_T * \left(T_{fracture} - T_f\right) * g_T\left(L, H, B_{temp.\,front}\right)$$

A_p = Poro-elastic constant (refer chapter 2.2)

A_T = Thermo-elastic constant (typically 100 kPa/°C), which can be expressed as

$$A_T = \alpha * \frac{E}{1-\nu}$$

α = Thermal expansion / contraction coefficient ($°C^{-1}$)

E = Young's modulus

ν = Poisson's ratio

$p_{fracture}$ = Pressure in the fracture

p_f = reservoir pressure

$T_{fracture}$ = Temperature in the cooled reservoir zone immediately around the fracture

T_f = Reservoir temperature

g_p , g_T = Geometry factors that depend on the fracture half-length L, its height H and the penetration depth of the injection water front ($B_{inj.\ front}$) or cooled zone front ($B_{cooled\ front}$), see Fig. 2.5. Note that both L and H and $B_{inj.\ front}$ / $B_{cooled\ front}$ depend on injection time.

Note that the thermo-elastic constant A_T is proportional to Young's modulus E. Therefore, for the same thermal expansion coefficient α, a stiffer rock will develop more thermo-elastic stresses as a result of cooling than a softer rock. This appears to be generally in line with field observations.

In the case of a propped hydraulic fracture stimulation, which is of relatively short duration, the pore pressure and temperature penetration depths into the reservoir are small, resulting in only a very small change in the overall stress level. However, for water injection fracturing the pore pressure and temperature penetration depths are significant, resulting in non-negligible poro-elastic and thermo-elastic stress changes around the fracture.

The net change in stress level will be dictated by the balance between the increased pore pressure and the decreased temperature. The overall change in the total stress is obtained by adding the individual changes to temperature reduction and pore pressure increase. To illustrate these effects, Fig. 2.6 shows changes in total stress owing to temperature decreases and pore pressure increases for a typical highly permeable North Sea sandstone after 2 years of high rate water injection.

In this case, temperature effects are dominating vis-à-vis the pore pressure effects, and the overall reduction in stress amounts to about 10% of the estimated minimum initial stress of 500 bar.

Figure 2.7 shows an example of the vertical distribution of these changes in total stress due to cooling, indicating that this effect basically remains confined to the reservoir due to limited heat conduction into the (impermeable) cap and base rock. This is tantamount to a stress barrier at the boundary between reservoir and cap and base rock, and hence a growing fracture may be confined against this barrier.

In contrast to the above example, water injection in a typical tight carbonate reservoir, can lead to increases in the overall total stress due to pore pressure increase which

outweighs the thermo-elastic stress decrease (Fig. 2.8). Thus, in this case, any initial stress barrier which may initially exist between the reservoir and cap rock may be eliminated after prolonged injection.

g) Formation impairment around the fracture (see refs. [18-20] for further background).

In spite of numerous efforts to date, no model exists that satisfactorily predicts the degree of formation damage induced by (produced) water injection as a function of oil/solids content, particle size distribution, etc. Therefore, our waterflood fracturing program adopts a very simple damage model, which contains a number of parameters that can be calibrated to laboratory tests and field tests. The effect of formation damage as a result of water injection under induced fracturing conditions has been taken into account by:

- An impaired zone around the fracture (see Fig. 2.5), which is characterised by a uniform degree of formation impairment
- An external filtercake on the fracture face with uniform permeability
- Internal plugging of the fracture

Below, each of these three points is discussed in further detail.

Impaired zone.

The impaired zone (see Fig. 2.5) is the formation area immediately adjacent to the fracture, which becomes impaired as a result of contaminated water injection. Laboratory experiments suggest that impairment of the formation around the fracture is largely the result of injected oil-in-water, plus some very small solids. Most injected solids do not penetrate into the formation. The residual formation permeability to water in the impaired zone has been measured to be approximately equal to the endpoint relative permeability to water. Therefore, the endpoint water relative permeability (input parameter) provides a good estimate for the 'damage factor' of this zone.

External filtercake.

Laboratory experiments also suggest that the injected solids make up an external filtercake, which covers the fracture face. The measurements indicate that the filtercake permeability is between 1 and 20 μD. The filtercake permeability appears to be lower for low-permeability rock and for heavy oil.

Internal plugging of the fracture.

Once external filtercake starts building up on the fracture face, conventional filtration theory predicts that no newly injected solids will be able to penetrate into the formation adjacent to the fracture. For a slowly growing fracture (as is the case for water injection) this may eventually result in a situation in which the filtercake thickness becomes approximately equal to the total fracture width, resulting in internal fracture plugging by injected solids. This is particularly applicabl to cases of very contaminated water injection into formations with very leak-off.

In such cases, the 'effective' fracture width could approach zero, resulting in very large frictional pressure drops. Within our waterflood fracturing program, the water flow in the fracture for thick filtercakes is assumed to be localised in 'wormholes', which form in the filtercake. Wormhole formation results in a significant reduction of the frictional pressure drop. The degree of internal fracture plugging at which wormholes start to form is provided by the user by means of the input variable f_{crit}. The variable f_{crit} is defined as the

ratio between the 'effective' frac width and the total frac width at which wormhole formation starts.

An order-of-magnitude value for f_{crit} may be estimated as follows. Consider the forces acting on an individual filtercake particle sitting on top of the external filtercake. Injected fluid flow towards the fracture tip will cause shear forces, and (leak-off) fluid flow perpendicular to the fracture face into the formation will cause normal forces. The shear forces tend to drag the particle away from the filtercake, whereas the normal forces tend to keep it where it is. The critical effective frac width at which a filtercake particle will start to be dragged away can be estimated by applying a standard slip criterion relating normal and shear forces acting on this particle. The result is

$$w_{crit}(r) = \sqrt{\frac{2k_e L}{D_{part} * f} \cos^{-1}\left(\frac{r}{L}\right)\sqrt{1-\left(\frac{r}{L}\right)^2}}$$

L = One-wing fracture length

k_e = External filtercake permeability

r = Distance away from the wellbore (in the fracture), $0 \le r \le L$

D_{part} = Diameter of the filtercake particle.

f = Slip coefficient. A value of $f \approx 10^{-3}$ has been estimated based on the results of earlier laboratory experiments.

The above equation shows that the critical effective frac width at which filtercake shearing starts increases proportionally with the square root of the fracture length. Since generally the *total* width w_{tot} of a propagating fracture also is approximately proportional to the square root of the fracture length, the ratio *fcrit* may be assumed independent of fracture length.

The above equation can also be used to estimate an order-of-magnitude value for f_{crit}. For a typical filtercake permeability of 10 μD, fracture length of 100 m and particle diameter of 1 micron, one obtains a value for w_{crit} in the order of 1 mm. For a 'typical' maximum water injection fracture width of ca. 10 cm, this implies a value for f_{crit} in the order of 0.01. This is of the same order as the value that was obtained by matching simulation to field data of produced water injection with very contaminated injection water.

2.4. Fracture containment

In most intervals to be fractured the formation is layered, with layers of heterogeneous rock properties, and the stress field exhibits gradients and discontinuities which influence the three-dimensional fracture propagation.

To date the following four factors have been identified in having a pronounced effect on vertical containment (all four can be addressed in our fracturing program):

- minimum in-situ stress contrast (see also under 2.4.d. above)
- Young's modulus (stiffness) contrast
- apparent fracture toughness (overpressure) contrast
- permeability contrast

Often contrasts in in-situ stresses and elastic properties are interrelated and occur simultaneously. A simple rule of thumb is that a stress contrast of more than 1000 psi (7 MPa) acts as a stress barrier and causes the fracture to be totally contained.

When a fracture runs into a zone of high leak-off it may become impossible for the fracture to penetrate that zone significantly, leading to an effective containtment by that zone.

The fracture geometry can be influenced in the completion stage by selective perforating. For instance, by specifying that the fracture should not break through the cap rock, the fracture length can be maximised by positioning the perforations in the bottom of the pay zone.

Geologic discontinuities such as faults, joints (natural fractures) and bedding planes, are frequently associated with discontinuities in in-situ stress. Consequently these discontinuities can also arrest lateral or vertical fracture propagation. This has been demonstrated in mine-back experiments, which also revealed that when a frac did propagate through a joint, an orientation change or the creation of multiple fractures took place. So far no method has been developed to quantify these effects via simulation.

3. EXAMPLE INPUT

Company name

Well name

Location

Date

Description Example case of water injection

Comments

INPUT

GEOLOGICAL MODEL

DepthTop (m)	LayerName
0	Overburden
990	Cap rock shale
1000	Injection zone
5000	Underburden

DepthTop (m)	DepthBottom (m)	LayerHeight (m)	StressTop (MPa)	StressBottom (MPa)	StressGrad (kPa/m)
0	990	990	0	15.64	15.8
990	1000	10	15.64	15.8	15.8
1000	5000	4000	15.8	79	15.8
5000	1e+004	5000	79	158	15.8

FormPresTop (MPa)	FormPresBot (MPa)	FormPresGrad (kPa/m)
0	9.9	10
9.9	10	10
10	50	10
50	100	10

ROCK PROPERTIES

DepthTop (m)	Permeability (md)	Porosity (-)	YoungModulus (MPa)	PoissonRatio (-)	FracToughnes (MPa*SQRT(m))
0	300	0.3	5000	0.25	1
990	1.5	0.03	5000	0.25	1
1000	300	0.3	5000	0.25	1
5000	300	0.3	5000	0.25	1

Fracture toughness exponent	-0.5	-

FORMATION PARAMETERS

Poro-elastic constant	0.6	-
Thermo-elastic constant	100	kPa/°C
GeoThermal gradient	0.03	°C/m
Reservoir temperature	50	°C

Reservoir temperature	50	°C
Heat capacity of rock	2560	kJ/(m³*°C)
Connate water saturation	0.3	-
Residual oil saturation	0.1	-
Total reservoir compressibility	1.5e-006	1/kPa
Formation fluid viscosity	0.5	mPa*s
Endpoint rel. perm. of oil	1	-
Endpoint rel. perm. of water	1	-

INJECTION FLUID & FILTER CAKE

Inj. water viscosity at inj. temp.	0.5	mPa*s
Inj. water viscosity at res. temp.	0.5	mPa*s
Inj. water heat capacity	4185	kJ/(m³*°C)
Inj. water density	1.02	g/cm³
Damage factor	0.1	-
Permeability	0.02	md
Fcrit	0.01	-
Kappa	1	-

FRACTURE DIMENSIONS

Init. fracture height upwards	1	m
Init. fracture height downwards	1	m
Init. fracture depth (TV)	1050	m
Init. fracture length	1	m
Max. fracture length	1000	m
Max. fracture height upwards	1000	m
Max. fracture height downwards	1000	m
Drainage radius	1500	m

WELLBORE HYDRAULICS

S# (-)	Description (-)	DepthBotAH (m)	DepthBotTV (m)	SectLengthAH (m)	SectLengthTV (m)
0		0	0	0	0
1		1050	1050	1050	1050

S# (-)	Description (-)	DepthBotAH (m)	InnerDiam (mm)	OuterDiam (mm)	FrictionMult (-)
0		0	0	0	1
1		1050	0	22.06	1

Init. fracture depth (AH)	1050	m

INJECTION CYCLES

InjTime (mon)	InjDuration (mon)	InjRate (m³/day)	SolidsLoadng (vol ppm)	OilLoading (vol ppm)	InjWatSurfT (°C)
0	240	1e+004	50	200	40

InjWatBHT (°C)
40.1

REFERENCES

1. G.Gheissary, P.A. Fokker, P.J.P. Egberts, F.J.T. Floris, G. Sommerauer and C.J. Kenter. Simulation of Fractures Induced by Produced Water Re-Injection in a Multi-Layer Reservoir. SPE 54735, presented at the SPE/ISRM Eurock '98 held in Trondheim, Norway, 8–10 July 1998.
2. P.J. van den Hoek. New 3D model for optimised design of hydraulic fractures and simulation of drill cuttings re-injection. SPE 26679, presented at SPE Offshore Europe, Aberdeen (1993).
3. Koning, E.J.L., Waterflooding under fracturing conditions, Ph.D. Thesis, Technical University of Delft, 1988.
4. Van den Hoek, P.J., Matsuura, T., De Kroon, M., and Gheissary, G.: "Simulation of Produced Water Injection Under Fracturing Conditions", SPE Prod. & Facilities 14 (3) August 1999, p. 166-176.
5. P.J. van den Hoek, G. Sommerauer, L. Nnabuihe, and D. Munro. Large-scale produced water re-injection under fracturing conditions in Oman. SPE 87267 (ADIPEC 0963), presented at Abu Dhabi Petr. Conference (2000).
6. P.J. van den Hoek, Z.I. Khatib, and G.J. Siemers. Causes of Injectivity Problems During Fractured Water Disposal and Their Remediation. SPE 74416, presented at SPE IPCEM, Villahermosa (2002).
7. M. Bai, S. Green, and P.J. van den Hoek. A parametric analysis of deep injection for waster disposal using a 3-D hydraulic fracture simulator (presented at NARMS conference, Toronto, 2002).
8. J.C. Noirot, P.J. van den Hoek, Dirk Zwarts, Hans Petter Bjoerndal, SPE, Rik Drenth, R. Al Masfry, B. Wassing, J. Saeby, M. Masoori, and A. Zarafi. Water Injection and Water Flooding Under Fracturing Conditions. SPE 81462, presented at SPE MEOS, Bahrain (2003).
9. S. Sathyamoorthy, P. Priyandoko, K.B. Flatval, A. Bulang, P.J. van den Hoek, and Y. Qiu. Radical Approach to Water Injection Scheme for Barton. SPE 84885, presented at SPE improved oil recovery conference in Asia Pacific, Kuala Lumpur (2003).
10. K.I. Ojukwu and P.J. van den Hoek. A New Way to Diagnose Injectivity Decline During Fractured Water Injection By Modifying Conventional Hall Analysis. SPE 89376, presented at SPE/DOE conference on improved oil recovery, Tulsa (2004).
11. B. Hustedt, Y. Qiu, D. Zwarts, and P.J. van den Hoek. Modeling Water-Injection Induced Fractures in Reservoir Simulation. SPE 95726, presented at SPE ATCE, Dallas (2005).
12. J. Sæby, H.P. Bjørndal, and P.J. van den Hoek. Managed Induced Fracturing Improves Waterflood Performance in South Oman. IPTC-10843, presented at IPTC, Doha (2005).
13. Hustedt, B., Qiu, Y., Zwarts, D., van Schijndel, L., and P.J. van den Hoek. The Impact of Water-Injection Induced Fractures on Reservoir Flow Dynamics: First Applications of a New Simulation Strategy. IPTC-10689, presented at IPTC, Doha (2005).
14. B. Hustedt, D. Zwarts, H.-P. Bjoerndal, R. Masfry, and P.J. van den Hoek. Induced Fracturing in Reservoir Simulations: Application of a New Coupled Simulator to Waterflooding Field Examples. SPE Reservoir Evaluation & Engineering Journal, Vol. 11 (June 2008), p. 569-576.
15. Van den Hoek, P.J., Al-Masfry, R., Zwarts,D., Jansen, J.D., Hustedt,B., and Van Schijndel, L. Waterflooding Under Dynamic Induced Fractures: Reservoir Management

and Optimization of Fractured Waterfloods. SPE Reservoir Evaluation & Engineering Journal, October 2009, p.671-682.

16. M. Khodaverdian, T.G. Sorop, P.J. van den Hoek, S.Sathyamoorthy and E. Okoh. Injectivity and fracturing in unconsolidated sand reservoirs: Waterflooding case study, offshore Nigeria. Paper Arma 10-139, prepared for presentation at the 44th US Rock mechanics Symposium and 5th US-Canada Rock mechanics Symposium, Salt Lake City, June 27-30, 2010.
17. M. Zwaan, R. Hartmans, S. Schoofs, B.R. de Zwart, G. Rocco, R. Adawi, F. Saadi, K. Shuaili, J. Lopez, J. Ita, T. L'Homme, T. Sorop, Y. Qiu, P.J. van den Hoek, F. Al-Kindy, S. Busaidi, and J. Fraser. EOR Field Management Through Well-Planned Surveillance. SPE 154620, presented at the SPE EOR Conference at Oil and Gas West Asia, Muscat, Oman, 16-18 April 2012.
18. L. Costier, P.J. van den Hoek, C. Davidson, Mei Ding, J.T.M. vanden Berg, R.A. Hofland. Establishing Water Injection Dynamics by Leading-Edge Coreflood Testing. SPE 121786. EUROPEC/EAGE Conference and Exhibition, 8-11 June 2009, Amsterdam, The Netherlands.
19. S. Aristov, P.J. van den Hoek and E. Pun. Integrated approach to manage formation damage in waterflooding. SPE 174174, presented at the 2015 SPE European Formation Damage Conference held in Budapest, Hungary, 3–5 June 2015.
20. S. Aristov, P.J. van den Hoek and E. Pun. Integrated approach to manage formation damage in waterflooding. Journal of Petroleum Technology, February 2017, p. 70-71.

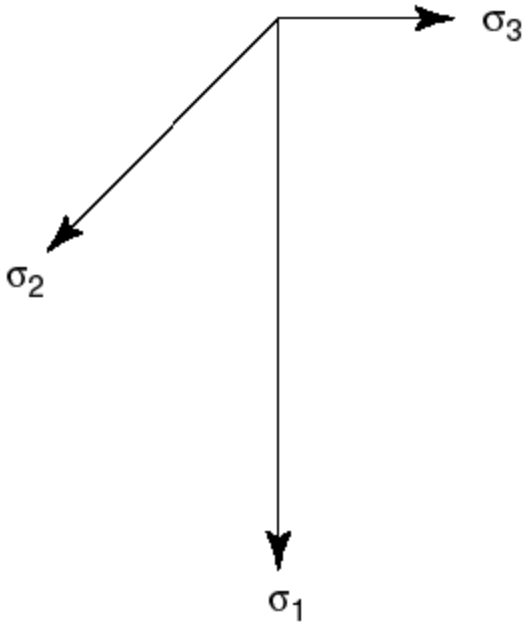

Fig. 2.1 In-situ Stresses ($\sigma_1 > \sigma_2 > \sigma_3$).

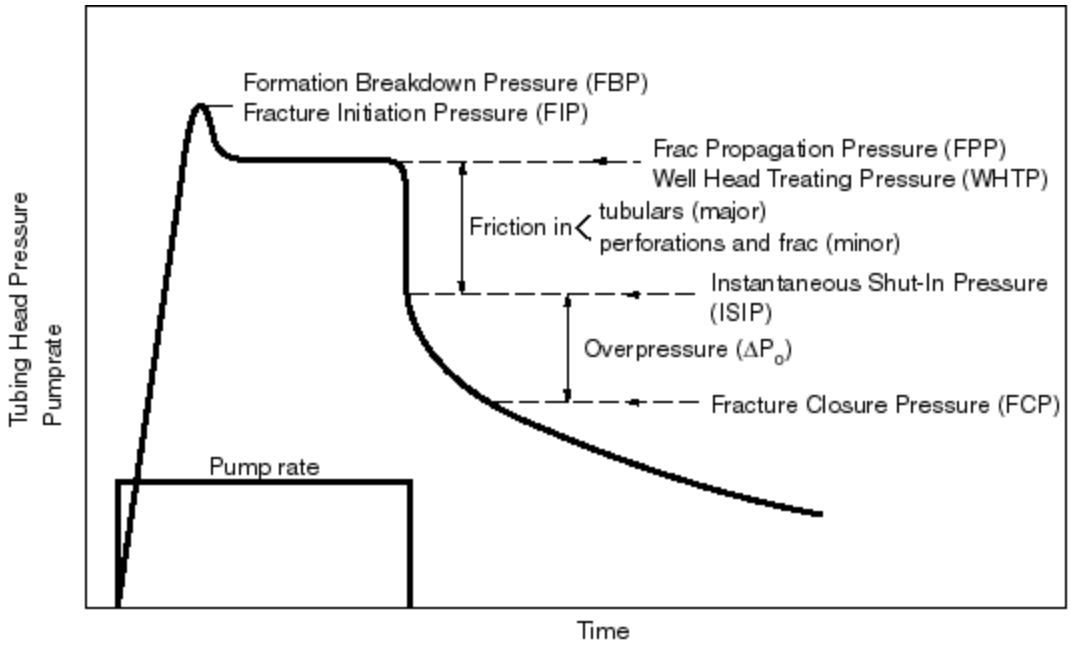

Fig. 2.2 Typical pressure response during fracturing.

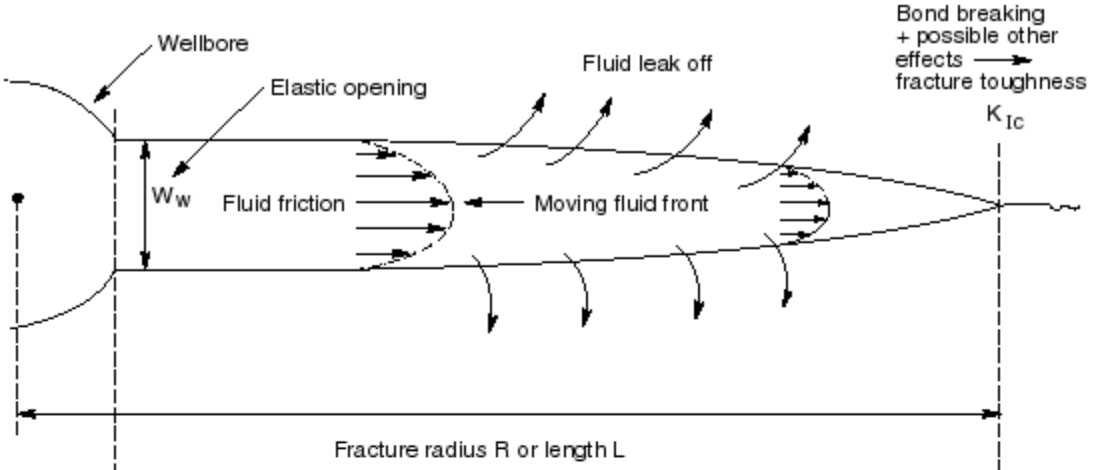

Fig. 2.3 (a) Schematic view of the physical processes going on in a propagating hydraulic fracture.

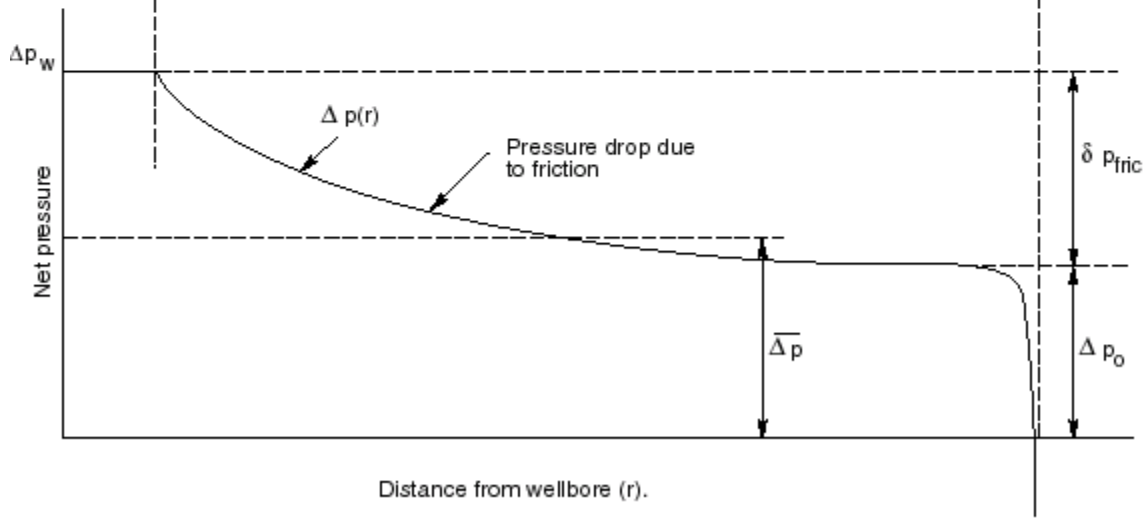

Fig. 2.3 (b) Qualitative plot of the fluid pressure distribution in a hydraulic fracture.

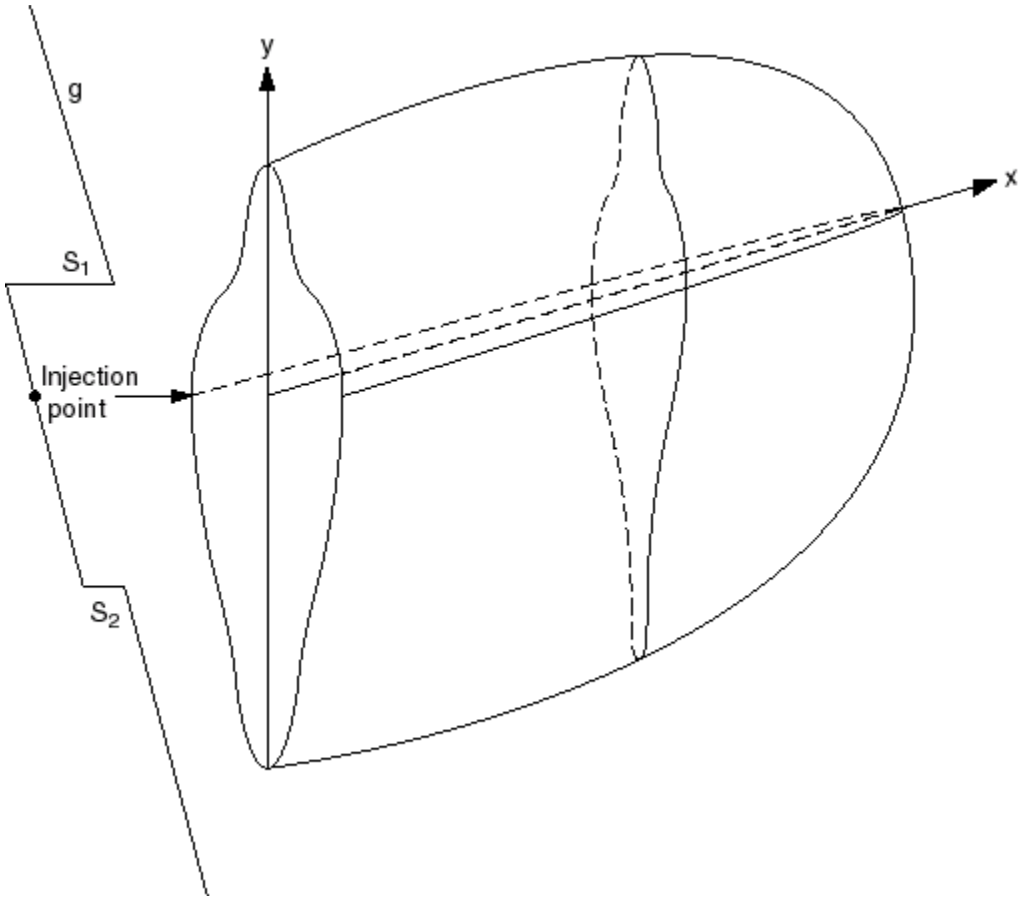

Fig. 2.4 Fracture geometry for a partially contained fracture.

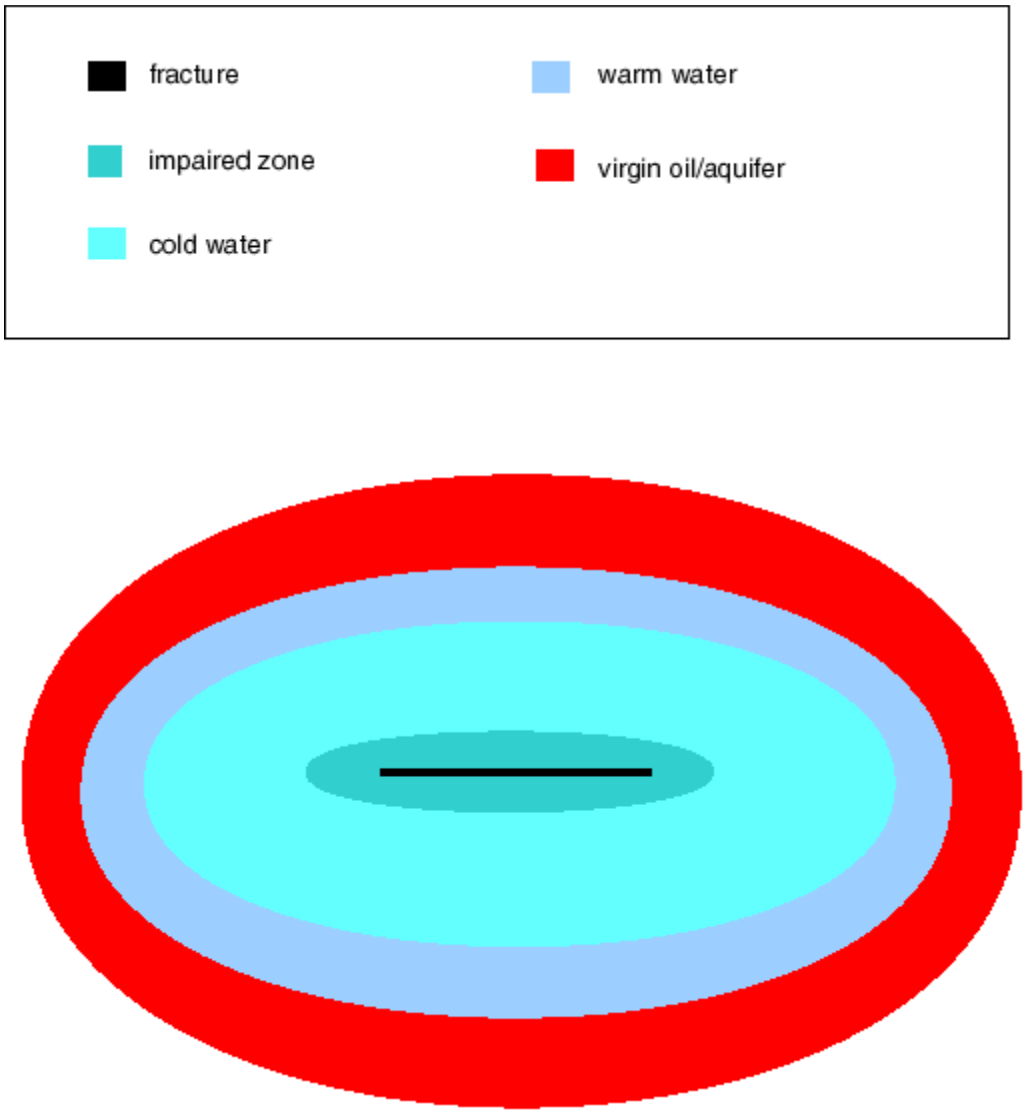

Fig. 2.5 Fracture surrounded by different mobility zones (schematic plan view)

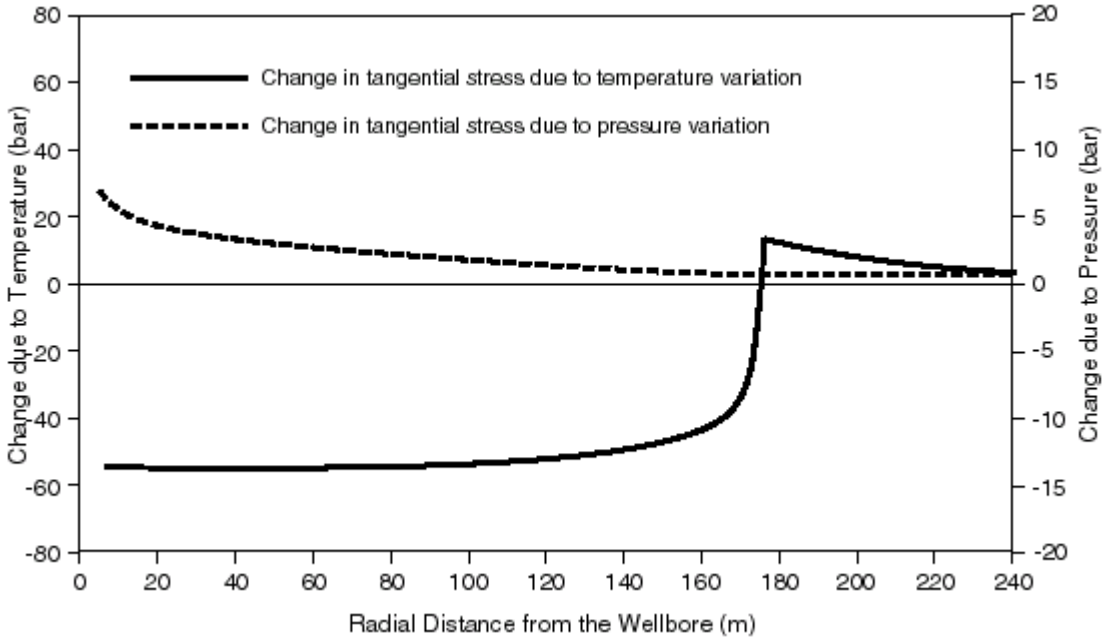

Fig. 2.6 Change in tangential stress due to pore pressure/ temperature alteration. (Sandstone reservoir)

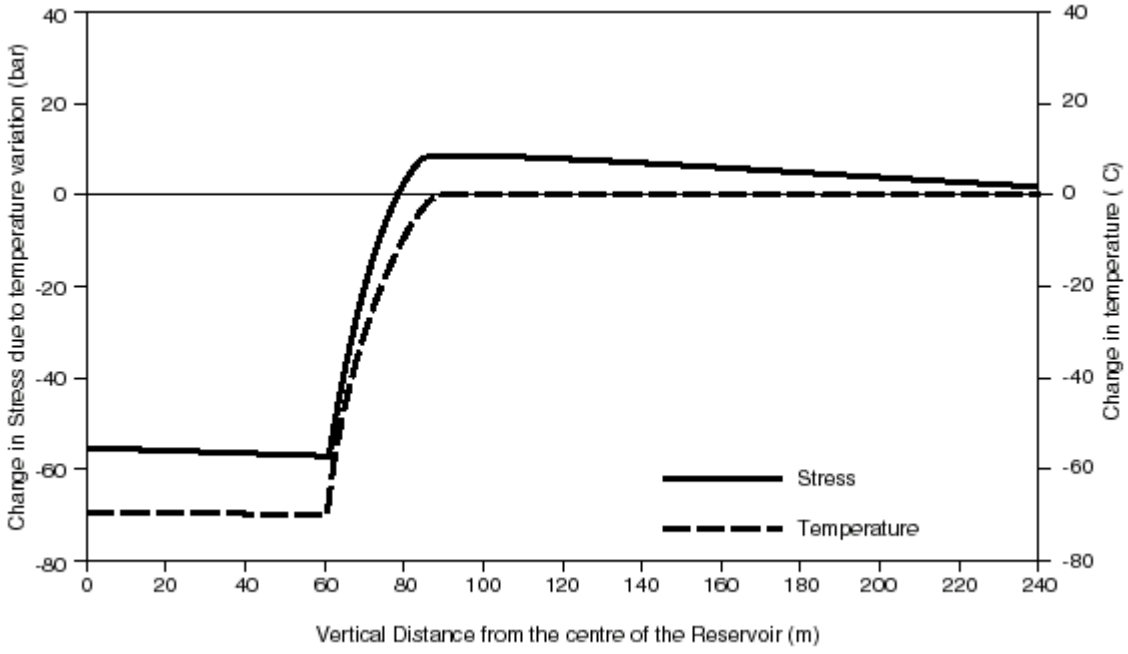

Fig. 2.7 Vertical temperature and stress distributions due to cooling. (Sandstone reservoir)

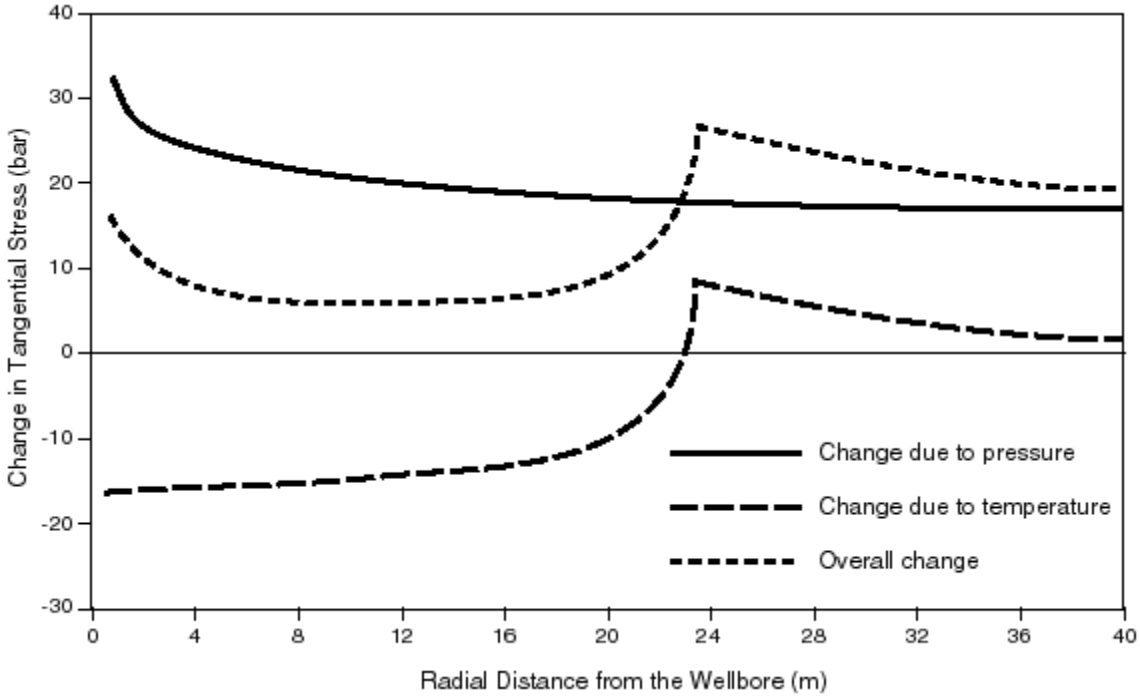

Fig. 2.8 Change in tangential stress due to pore pressure/ temperature alteration. (Limestone reservoir)